Short-Time Fourier Transform Analysis of Current Charge/Discharge Response of Lithium-Sulfur Batteries

Journal of The Electrochemical Society, 2023 **170** 110511
1945-7111/2023/170(11)/110511/6/$40.00 © 2023 The Electrochemical Society ("ECS"). Published on behalf of ECS by IOP Publishing Limited

Short-Time Fourier Transform Analysis of Current Charge/Discharge Response of Lithium-Sulfur Batteries

Anis Allagui,[1,2,3,z] Osama Awadallah,[3] Bilal El-Zahab,[3] and Chunlei Wang[4]

[1]*Department of Sustainable and Renewable Energy Engineering, University of Sharjah, PO Box 27272, Sharjah, United Arab Emirates*
[2]*Center for Advanced Materials Research, Research Institute of Sciences and Engineering, University of Sharjah, PO Box 27272, Sharjah, United Arab Emirates*
[3]*Department of Mechanical and Materials Engineering, Florida International University, Miami, Florida 33174, United States of America*
[4]*Department of Mechanical and Aerospace Engineering, University of Miami, Coral Gables, Florida 33146, United States of America*

Measurements acquired on batteries in the form of time signals such as voltage-time and capacity-time to assess their cyclability performance can be supplemented by examining their frequency-domain response. This allows one to determine the global characteristics of the signals and the battery, but not the local behavior, which is very important for determining for example battery fading. In this study we examine the short-time Fourier transform for time-frequency deconstruction of galvanostatic charge/discharge signals of lithium-sulfur batteries, taken as an example. The results displayed in terms of spectrograms show how the frequency content of such signals (e.g. charge and voltage time series) evolve with the lifetime of the batteries allowing the detection of critical changes in the response that may lead to fading and eventually default.
 [DOI: 10.1149/1945-7111/ad07ad]

Manuscript submitted July 13, 2023; revised manuscript received October 5, 2023. Published November 8, 2023.

Considering the ever-growing demand and usage of electrochemical energy storage devices and systems, their importance in our daily lives cannot be overestimated.[1] Batteries and supercapacitors of different types and chemistries, geometries and sizes are omnipresent around us, and can be found in virtually all consumer electronics, in portable medical devices, electric vehicles, uninterrupted power supplies, and emergency backup systems.[2–5] As such, from an electrical perspective, the types of loads expected to be powered by these devices vary widely from high-power demanding loads to high-energy demanding ones, from constant current, voltage or power loads to others with intermittent dynamics, and therefore with different temporal and frequency features.[6–8] Furthermore, these devices are intrinsically dissipative and time-evolving systems.[9] For the case of batteries for instance, capacity fading is known to be due to thermal dissipation and the existence of irreversibilities of different nature, such as electrolyte decomposition and evaporation, chemical mixing, formation of new phases, and volumetric expansion which all cause continuous and unavoidable performance decay.[10–12] Similarly, undesirable redox reactions in supercapacitors especially when over-charged or over-heated lead to the degradation of the electrodes and release of detached particles into the electrolyte, which in turn cause the reduction of effective surface area of the electrodes and increased obstruction of ions movement. In addition, internal over-pressure due to the formation of gaseous species can cause electric contact loss which accelerates the wear-out and even explosion of the cell.[13–15] Hence, time representations of the electrical signals of batteries and supercapacitors are usually insufficient to fully describe their long-term cycling performance as they just present how the signal's amplitude changes in the course of time. That is why frequency-domain analysis is commonly employed as a supplementary analytical tool which tells us how often these amplitude changes take place. We recall that frequency-domain analysis of signals is nothing but an indirect way of looking at the same time-domain signals using time-to-frequency transformations such as the Fourier transform, Laplace transform, or other similar techniques. However, with the frequency-domain impedance spectroscopy technique for instance, all temporal information of the signal is lost given that the analysis is not associated with any particular instant in time. The same can be said when thecharacterization is performed in the time domain using galvanostatic charging and discharging for example, which does not provide any information about the frequency behavior. In other words, while these two dual representations enable the understanding of the global characteristics of signals in one domain or another, but separately, they are not suitable for analyzing local properties, especially when the device's response exhibits time-evolving frequency contents.[16]

This leads us to the motivation behind this work in which we apply joint time-frequency analytical tools to time-domain electrical signals of lithium-sulfur (Li-S) batteries (taken as an example) especially when one is interested in evaluating the performance of the device under cyclic operation. Cyclability is especially relevant for applications in which the energy storage device is required to undergo hundreds or thousands of sequences of deep discharges followed by recharge to maximum capacity,[17–19] such as in consumer devices and load leveling systems. Such tests are usually performed by subjecting the device to extended cycling of square wave (power, current or voltage) signals with control on the lower and upper voltage limits, and then observing the capacity retention vs cycle number and variation of internal resistance.[20] Charging using constant current-constant voltage (CC-CV) input and discharging via constant power is also a commonly used scheme for long term performance tests of these devices. Furthermore, the coulombic efficiency, which is calculated as the ratio of discharged capacity by the stored capacity for each cycle, can be used as an indicator of how reversible the process is. For the case when the charge and discharge are performed at the same current rate, the coulombic efficiency is also equal to ratio of discharge time by the charge time for each cycle. Because of ageing and degradation of performance as outlined above, the amounts of stored or released charge between the two voltage limits are reduced with the increase of cycles, and therefore the signals are not periodic with a constant frequency anymore, but rather time-variant. In other words, the time durations of cycles keep decreasing as the device is being charged and discharged, which makes plots vs cycle number not representative of the full picture. A joint time-frequency analysis is more appropriate to monitor and understand the dynamics of the devices in these conditions. To the best of our knowledge, apart from a brief introduction of the technique in a previous work of ours,[21] this is the first report on time-frequency decomposition and analysis of battery signals in response to constant current charge/discharge (between two voltage limits) until complete capacity fading.

[z]E-mail: aallagui@sharjah.ac.ae

There are several techniques for representing a one-dimensional time-domain signal in the combined two-dimensional time-frequency plane. These methods can be linear or nonlinear, parametric or nonparametric, etc., and include for instance the short-time Fourier transform (STFT), the wavelet transforms, the Hilbert method, the Wigner-Ville method, and others.[22] We note that many time-frequency analyses result inevitably in some loss of signal, which makes it not possible to reconstruct the original time series signal perfectly from the results of the time-frequency decomposition. However, new qualitative and/or quantitative knowledge of the characteristics of the signal are probably more important than being able to revert back to the original perfectly. In other words, while some signal may be lost in the computational process, new information can be gained about the original signal. Our focus in this study is to introduce the concept for characterizing the cyclic electrical behavior of batteries via the Fourier-type time-frequency analysis which is the classical method of time-frequency analysis. It has been found very helpful for analyzing nonstationary seismic signals, sound and speech signals, physiological signals linked to the cerebral activity and the cardiac system, Raman spectra, etc.[16,23] We focus on the response of Li-S batteries to successive constant current charging/discharging sequences between two lower and upper voltage limits in order to visualize the signals of certain electrical quantities (voltage and charge) in the form of a time-frequency map from which one can detect or estimate any remarkable behavior. Optimization to reduce, for instance, interference and improve the readability of the maps is not the purpose of this study.

Theory and Methods

Battery data.—The joint time-frequency decomposition of time-domain signals $x(t)$ (e.g. charge and voltage time series in response to symmetric galvanostatic charge/discharge between two voltage limits) by STFT will be applied on data collected from Li-S batteries, fabricated and assembled as follows. First, the cathode material was prepared by mixing together 63% of sulfur, 32% of carbon, and 5% of binder. Cathode slurry of different sulfur loadings was doctor blade-coated on aluminum foil, and then dried at 60 °C. For the anodic side, we used a 250 μm thick lithium foil. A polypropylene membrane was employed as a separator. As for the electrolyte, it was prepared by dissolving 1 mol L^{-1} of lithium bis (trifluoromethanesulfonyl)imide (LiTFSI) and 0.1 mol L^{-1} of lithium nitrate ($LiNO_3$) in a mixture of 1,3-Dioxolane (DOL)/1,2-Dimethoxyethane (DME) (1:1 v/v) solution. Coin cells type CR2032 were assembled inside a glove box filled with argon gas, and subsequently cycled with symmetric galvanostatic charge/discharge waveforms.

In this study, two battery cells with different sulfur loadings were tested at different (initial) C-rates. The C-rate are estimated based on the theoretical capacity of 1675 mAh/g-sulfur. The actual sulfur loading was determined by thermogravimetric analysis (TGA). Li-S cells with 3.40 mg cm^{-2} loading were cycled at a C-rate of C/5 for both charge and discharge sequences. Other cells prepared with sulfur loading of 4.20 mg cm^{-2} were tested at a C-rate of C/10 for both charge and discharge. All cells were cycled within the voltage window of 1.80–3.00 V. We applied the same C-rate of galvanostatic charge and discharge as it provides voltage and capacity signals relatively easy to interpret in the joint time-frequency domain. But in principle, non-symmetric waveforms can also be evaluated.

Short-time Fourier transform.—In this section we review the basics of the STFT, which is considered to be the classical technique that allows a signal representation in the time-frequency plane. The STFT of a signal $x(t) \in L^2(\mathbb{R})$ is defined using an analysis window $g(t)$ by the linear transformation:[16,24]

$$\mathrm{STFT}_x^g(t,f) = \int_{-\infty}^{\infty} x(t')g^*(t'-t)e^{-j2\pi ft'}dt' \quad [1]$$

which is the Fourier transform (defined as $X(f) \coloneqq \int_{-\infty}^{\infty} x(t)e^{-j2\pi ft}dt$) of the windowed signal, i.e. the product $x(t')g^*(t'-t)$. It is clear that while $x(t)$ is a function of time t, its $\mathrm{STFT}_x^g(t,f)$ is a function of both time t and frequency f. The associated reconstruction or synthesis formula is:

$$x(t') = \frac{1}{2\pi}\int_{-\infty}^{\infty}\int_{-\infty}^{\infty} \mathrm{STFT}_x^g(t,f)\gamma(t'-t)e^{j2\pi ft'}dfdt \quad [2]$$

with the condition that $\int_{-\infty}^{\infty} g^*(t')\gamma(t')dt' = 1$.[16,24] The analysis window $g(t)$ is (generally) an even, real-valued function concentrated around time zero where it is maximum, and its Fourier transform is (generally) concentrated around the zero frequency where it is maximum. The window suppresses the signal $x(t)$ outside a certain region, and its Fourier transform yields a local spectrum.[24] Moreover, $g(t)$ is supposed to be normalized in $L^2(\mathbb{R})$ (i.e. $E_g = \int_{\infty}^{\infty}|g(t)|^2dt = 1$), and with compact support. The term $g(t'-t)e^{j2\pi ft'}$ represents the collection of all time and frequency translations of the window g or the family of time-frequency atoms which are localized in the time-frequency plane in $[t-\Delta t_g/2; t+\Delta t_g/2] \times [f-\Delta f_g/2; f+\Delta f_g/2]$, where Δt_g and Δf_g are the time and frequency spreads.[16] It is known from Heisenberg uncertainty principle that it is not possible to maximize both the temporal resolution and frequency resolution simultaneously. Choosing a narrow time window for good time resolution implies a poor frequency resolution, and vice versa, a wide time window and thus poor time resolution implies improved frequency resolution. The lower limit on the area of the rectangle representing the time-frequency localization of an atom is given by the inequality $\Delta t_g \Delta f_g \geqslant 1/(4\pi)$.[16]

Since the STFT of the signal is complex-valued in general, we often use the spectrogram for display purposes, as we show below. From $\mathrm{STFT}_x^g(t,f)$, the energy of $x(t) \in L^2(\mathbb{R})$ can be calculated from :[16]

$$E_x = \int_{-\infty}^{\infty}|x(t)|^2dt = \int_{-\infty}^{\infty}\int_{-\infty}^{\infty}|\mathrm{STFT}_x^g(t,f)|^2df\ dt \quad [3]$$

where the squared magnitude of the STFT of $x(t)$, i.e.:

$$S_x^g(t,f) = |\mathrm{STFT}_x^g(t,f)|^2 \quad [4]$$

is the spectrogram of $x(t)$. It defines a time-frequency map of the signal and can be viewed as a quantity measuring at each instant a spectral density of local energy of $x(t)$. A schematic illustration of the different computational steps needed to obtain the spectrogram of a signal using STFT is shown in Fig. 1.

All signal processing methods and associated graphs presented in this work were carried out and plotted using MATLAB ver. R2019b (with Signal Processing Toolbox) on a personal computer, MacBook Pro, 2.2 GHz 6-Core Intel Core i7.

Results and Discussion

Li-S battery at C/10 rate.—Results and analysis of data obtained on the Li-S battery subjected to initial C/10 charging/discharging rates are shown in Fig. 2. The data were processed as-is without the application of any pre-conditioning algorithms of the type smoothing, filtering or detrending for example.

First, we show in Figs. 2a–2c the current (steps of 1 and −1 mA), capacity (in mA.h) and voltage (in V) time series at different days of measurements, i.e. at the beginning (up to the end of day 2) and

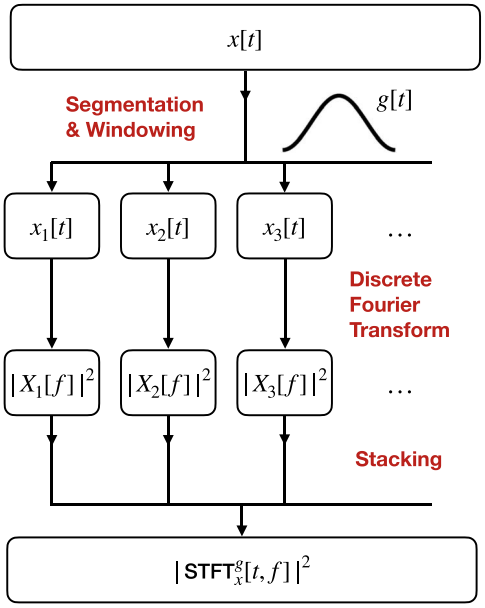

Figure 1. Flowchart of the computational steps for obtaining the spectrogram $|\mathrm{STFT}_x^g[t,f]|^2$ of a time-domain signal $x[t]$ via the short-time Fourier transform (STFT).

close to the end of the battery lifetime (around days 16-18), and at a certain point in time in between (around days 12-14). The time step of excitation and measurement was set to 5 s. We can see qualitatively from the figures that the frequency of charging/discharging current waveform applied on the battery, with the resulting capacity and voltage signals increase slightly with time. This is the result of gradual capacity fading of the battery. Although the changes are minimum for this case, such types of signals are globally non-periodic, and are described as time-varying or nonstationary signals because their frequency content varies with time. Figure 2d illustrates such changes in terms of accumulated capacities during the charge and discharge sequences as a function of cycle number. It is clear that the rates of changes of capacities are relatively slow until the very end of the cyclic lifetime of the battery where an abrupt collapse in capacity can be observed. We note here that the durations of successive cycles of charge/discharge cannot be constant, and thus information about the time is lost from such types of representations. Plots of the autocorrelation functions of the three time series signals of current, capacity and voltage defined as :[26]

$$r[k] = \frac{\frac{1}{T}\sum_{t=1}^{T-k}(x[t]-\bar{x})(x[t+k]-\bar{x})}{\sum_{t=1}^{T}\frac{(x[t]-\bar{x})^2}{T}} \qquad [5]$$

are shown in Fig. 2e for up to a lag $k = 200$ (time step is 5 s). Here $\{x_1, x_2,\ldots,x_T\}$ are the T successive values of the measured current, capacity or voltage time series, and $\bar{x} = T^{-1}\sum_{t=1}^{T} x[t]$ is the sample mean. The decrease in the samples autocorrelation coefficients values from one as the lag k is increased is another way to visualize that the measured electrical signals are nonstationay in time.

The frequency content of these signals (not the change in frequency content with time) can be assessed from a spectral point of view using the discrete Fourier transform (DFT, via Fast Fourier Transform (FFT) algorithm) applied to the entirety of the signals, knowing again that such technique does not allow an assignment of spectral components to time. The spectral representation of a signal $X(f)$ indicates which frequencies are present in the time-domain signal $x(t)$ with their relative magnitudes, the minimum and maximum frequencies and the bandwidth resulting from their difference.[22] In Fig. 2f, we plot the power spectra in dB vs frequency from 0 to 100 mHz for the current, charge and voltage records. The results indicate that, on top of the very low frequencies close to zero Hz associated with the fundamental frequencies of the quasi-square wave current input, triangular-like capacity and the associated voltage signal, higher frequency contents are also present. Such high-frequency parts of the signal gain in magnitude as the battery is charged/discharged faster and faster as we get close to its lifetime limit. However, no quantitative indication of how the frequency content of the signals changes with time can be derived from the traditional Fourier analysis, which is in general an important information for nonstationary signals. This is because the traditional Fourier transform requires the variables t and f to be mutually exclusive, and the evaluation of one value for $X(f)$ at a frequency f requires the knowledge of $x(t)$ for all values of t (recal l that $X(f) \coloneqq \int_{-\infty}^{\infty} x(t)e^{-j2\pi ft}dt$), i.e. time is integrated out of $X(f)$. But in our case, there is a time-dependency of the signal frequency spectrum, or equivalently time-dependency of the signal autocorrelation function as shown in Figs. 2a- 2c and in Fig. 2f, respectively.

Again, because of the mentioned-above limitations of separate time-domain or frequency-domain representations in analyzing nonstationary signals, we present in Figs. 2g–2i the STFT spectrogram representations (discrete version of Eq. 4) of current, capacity and voltage time series of the battery under test. The spectrogram is a three-dimensional graph wherein the x-axis represents time, y-axis represents frequency and the colored map represents the joint time-frequency power of the signal in dB (each pixel of area $\Delta t_g \Delta f_g$ is assigned a color). A cross-section at a constant t should show the frequencies present at the time t, and a cross section at a constant f should show the times at which the frequency f is present. In a way, the spectrogram representation consists of stitched DFT results after being applied to a number of adjacent slices of time series data similar to those shown in the three subfigures, Figs. 2a–2c. Each of these short sub-signals, assumed to be stationary in their respective time frames, are multiplied with an appropriate window in order to reduce the effect of leakage due to the time truncation of the signal, and then DFT is applied to each segment. Again, Fig. 1 illustrates the sequences of computational steps for STFT time-frequency decomposition. For the computation of the results shown in Figs. 2g- 2i the time resolution is set to 4.83 min, with a frequency resolution of 5 mHz and using a approximate of a Hann window (leakage = 0.85).[16,25] These values for the time and frequency resolutions were obtained after several trials, and are deemed fine enough to resolve (and display in the spectrograms) possible changes in the signals under test. Overall, the STFT spectrograms in this case do not show a distinctive variability in the time-frequency power representation as the battery is being continuously charged and discharged. Each slice in time from zero till day 18.9 appears to be similar to the next, which is expected and justified by the slowly varying profile of capacity vs cycle number plotted in Fig. 2d. The highest power concentration is observed for the very close-to-dc frequencies corresponding to the quasi-square waveform of the current and the resulting charge and voltage signal. Some vertical ridges at different higher frequency points can also be seen, which correspond to the changes in magnitudes of some DFT components as illustrated by Fig.2e. From this point of view, and using the spectrogram settings above, one cannot easily assess the capacity fade dynamics of this battery or predict in advance when a failure is to be expected.

However, a zoom between 18.959 and 18.963 on the x-axis (in days) shows the expected abrupt change in frequency content for all current, charge and voltage spectrograms (Figs. 2j–2l). The change occurred in a way such as now (between day 18.961 and 18.962) higher frequency components are contributing to the signals, which means that the battery's charge and discharge sequences are happening faster and faster, and thus less amount of energy storage and delivery. This instance in time points out to the transition from the quasi-flat response observed in most of Fig. 2d to the complete depletion and death of the battery that took place over the last two or three cycles of operation.

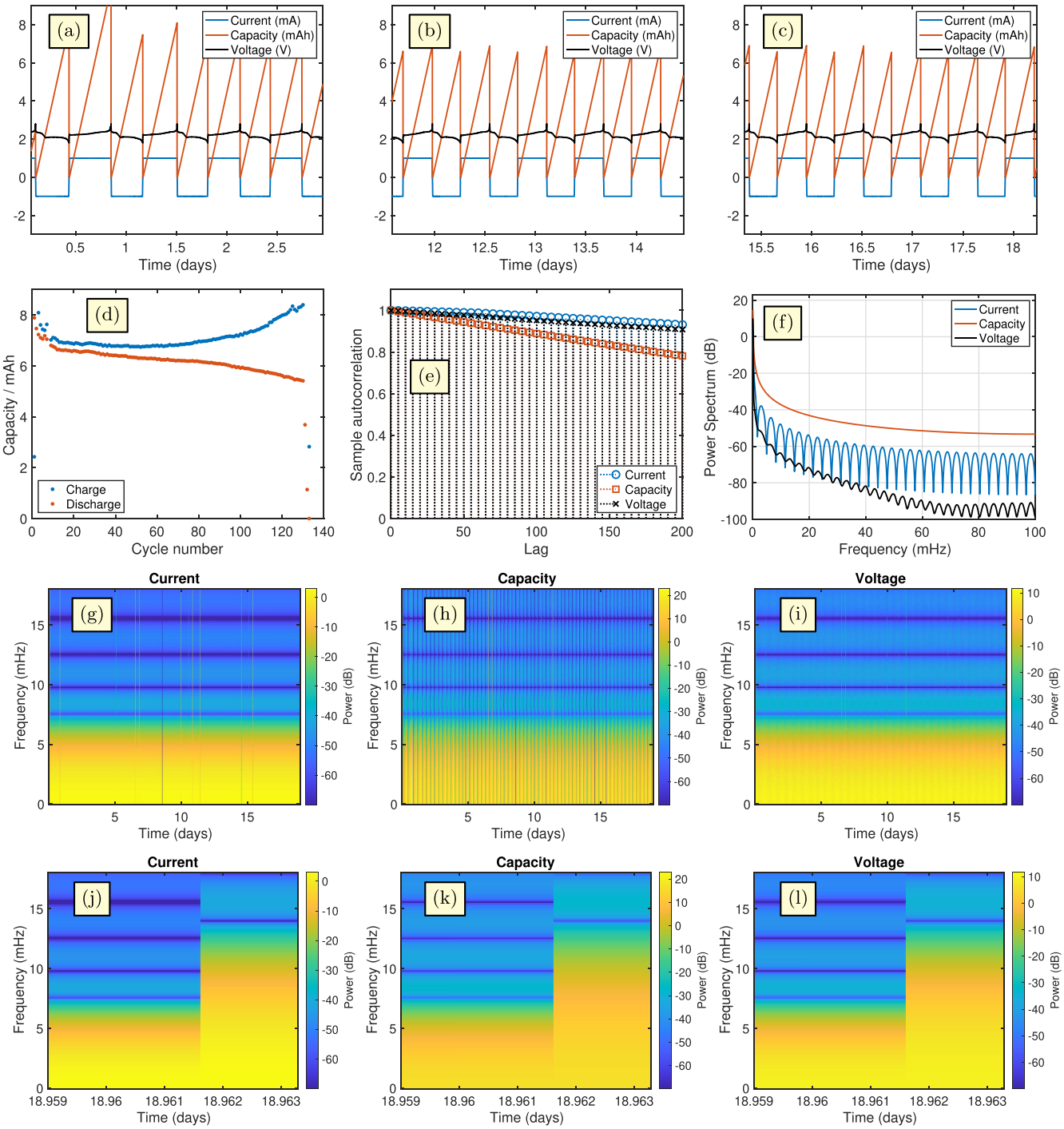

Figure 2. Experimental and computational results for the Li-S battery charged/discharged at C/10 rate between 1.80 and 3.00 V: (a), (b) and (c) Current (in mA), capacity (mA.h) and voltage (in V) time series collected at different time intervals. (d) Charge and discharge capacities as a function of cycle number. In (e) we show plots of autocorrelation coefficients of current, capacity and voltage signals for up to a lag of 200 pts (time step is 5 s), and in (f) the power spectrum of the full current, capacity and voltage signals using Kaiser windowing,[25] leakage = 50%. STFT spectrograms of the full signal of (g) current, (h) capacity and (i) voltage; Frequency resolution = 5 mHz, Time resolution = 4.83 min, Overlap percent = 50 %, leakage = 0.85 (approximates windowing the data with a Hann window[25]). (j), (k) and (l) are spectrograms (g), (h) and (i) respectively zoomed close to the end of the battery lifetime.

We should note at this point that establishing explicit connections between the time-frequency maps of system-level electrical signals and the common physical phenomena associated with capacity fade in Li-S batteries (e.g. active material loss from the cathode, irreversible sulfur species formation, parasitic reactions like the shuttle mechanism, and chemical reactions leading to self-discharge) is not straightforward and requires further detailed investigations.

Li-S battery at C/5 rate.—In a similar way for time-domain, frequency-domain and time-frequency domain data analysis presented above, the results obtained from the second battery tested for this study, i.e. Li-S with C-rate of C/5, are summarized in Fig. 3. Much different from the case of Li-S battery charged/discharged at C/10, time-domain plots (time step is 10 s in this case) of current (between 2.47 and −2.47 mA), charge and voltage (Figs. 3a–3c) and their

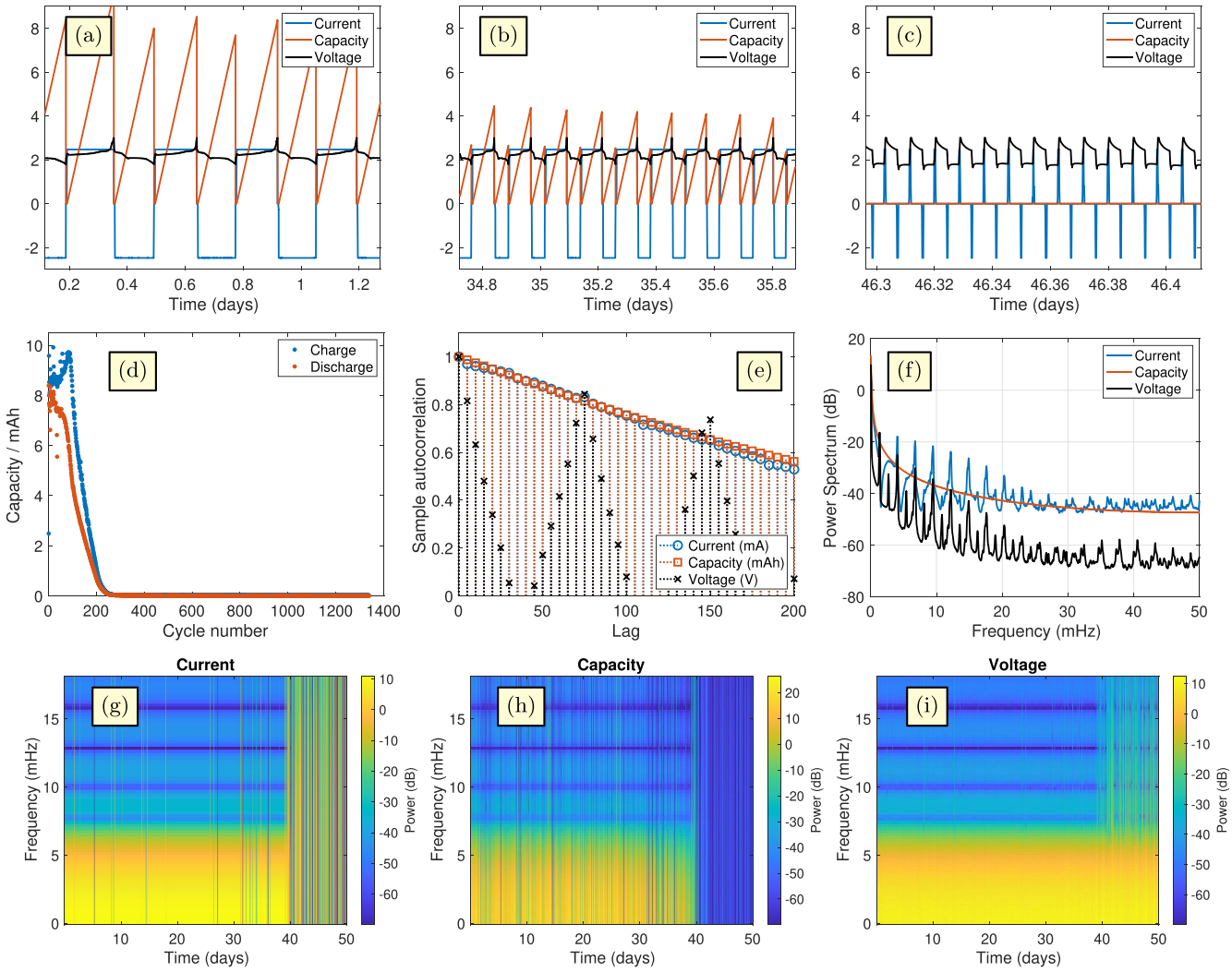

Figure 3. Experimental and computational results for the Li-S battery charged/discharged at C/5 rate between 1.80 and 3.00 V: (a), (b) and (c) Current (in mA), capacity (mA.h) and voltage (in V) time series collected at different time intervals. (d) Charge and discharge capacities as a function of cycle number. In (e) we show plots of autocorrelation coefficients of current, capacity and voltage signals for up to a lag of 200 pts (time step is 5 s), and in (f) the power spectrum of the full current, capacity and voltage signals using Kaiser windowing,[25] leakage = 50%. STFT spectrograms of the full signal of (g) current, (h) capacity and (i) voltage; Frequency resolution = 5 mHz, Timeresolution = 4.83 min , Overlap percent = 50 %, leakage = 0.85 (approximates windowing the data with a Hann window[25]).

respective correlation functions plots (Fig. 3e) indicate a clear nonstationarity of the data, and a more noticeable change of frequency content with time. Looking at the data reported in Figs. 3b and 3c compared to the data of day 1 (Fig. 3a), there is no doubt that the battery is getting close to its limit in terms of energy storage and delivery capability. The capacity in Fig. 3c is practically zero. The same conclusions can be drawn from the spectral power plots (Fig. 3f), wherein components from a relatively wide frequency bandwidth away from dc are contributing with stronger magnitudes for the three time series signals. Charge/discharge capacities vs cycle number (see Fig. 3d) confirm these observations, but again with loss of temporal information on the battery dynamics given that the duration of successive cycles gets shorter and shorter with time.

The STFT spectrograms shown in Figs. 3g–3i using the same computational settings as for Figs. 2g–2i clearly demonstrate for this battery how the current, capacity and voltage time series start to drastically change from about 40 d of charge/discharge onward, which is an indicative sign of gradual cell capacity degradation. This was not the case for the Li-S battery charged/discharged at C/10 which suddenly reached its lifetime limit without prior warning. However, readjusting and optimizing the frequency and time resolutions (i.e. different time-frequency maps) would allow one to capture easier any changes in behavior. These parameters are left to the user or an automated routine to define depending on the wanted precision in determining any change of dynamics of the battery. Looking closely at the capacity spectrogram in Fig. 3 h, we observe that from day 40 and beyond all frequency components are weakly represented which correspond to the relatively flat spectrum of the very low value of capacity centered at about 0.006 mAh. Just before day 40, one can observe a gradual decrease in the power assigned to the low frequencies, say from 0 to 5–6 mHz, which can be used as a metric to determine the change in state-of-health and capacity degradation of the battery. The same conclusions can be drawn from the analysis of the current and voltage spectrograms.

Conclusion and Outlook

Time-domain representations of electrical quantities such as voltage or charge, or frequency-domain impedance characterization of batteries cannot show the change in frequency content with time, and thus the evolution dynamics of the battery behavior as it is being used. However, this is an important information to know in order to detect any anomaly in its response or determine at what point in time the battery starts transitioning toward critical health situations. We

presented in this study how the joint time-frequency analysis of nonstationary time series applied on data collected from two Li-S batteries (taken as examples) can be used as a reliable tool for accurate monitoring of their state of health, state of charge, and capacity degradation. We used the standard STFT as a decomposition technique of 1D time-domain signals into 2D time-frequency maps, and the STFT spectrogram (squared modulus of the STFT) for data processing and interpretation. But in principle other time-frequency mapping operators such as the continuous wavelet transform can be applied. The spectrograms, with certain temporal and frequency resolutions, provide meaningful features on the battery behavior that cannot be otherwise detected from separate time or frequency analyses of the signals. For instance, for the case of the Li-S battery operated at C/5 rate in this study, the capacity spectrogram shows a gradual decrease in the power assigned to the low frequencies below 5 mHz, which can be used as a quantitative measure to assess the actual characteristics of the battery.

Acknowledgments

A.A. and C.W. acknowledge the support provided by the NSF, project #2126190. O.A. and B.E. are financially supported by Lion Battery Technologies Inc.

ORCID

Anis Allagui https://orcid.org/0000-0001-6044-9158
Chunlei Wang https://orcid.org/0000-0003-2574-7314

References

1. Z. Bassyouni, A. Allagui, and J. D. Abou Ziki, "Microsized electrochemical energy storage devices and their fabrication techniques for portable applications." *Adv. Mater. Technol.*, **8**, 2200459 (2023).
2. A. Sumboja, J. Liu, W. G. Zheng, Y. Zong, H. Zhang, and Z. Liu, "Electrochemical energy storage devices for wearable technology: a rationale for materials selection and cell design." *Chem. Soc. Rev.*, **47**, 5919 (2018).
3. Y. Jiang, J. Fletcher, P. Burr, C. Hall, B. Zheng, D.-W. Wang, Z. Ouyang, and A. Lennon, "Suitability of representative electrochemical energy storage technologies for ramp-rate control of photovoltaic power." *J. Power Sources*, **384**, 396 (2018).
4. A. Lahyani, P. Venet, A. Guermazi, and A. Troudi, "Battery/supercapacitors combination in uninterruptible power supply (ups)." *IEEE Trans. Power Electron.*, **28**, 1509 (2012).
5. A. Allagui, A. S. Elwakil, M. Fouda, and A. G. Radwan, "Capacitive behavior and stored energy in supercapacitors at power line frequencies." *J. Power Sources*, **390**, 142 (2018).
6. A. Allagui, M. Fouda, and A. S. Elwakil, "The ragone plot of supercapacitors under different loading conditions." *J. Electrochem. Soc.*, **167**, 020533 (2020).
7. M. E. Fouda, A. Allagui, A. S. Elwakil, A. Eltawil, and F. Kurdahi, "Supercapacitor discharge under constant resistance, constant current and constant power loads." *J. Power Sources*, **435**, 226829 (2019).
8. A. Allagui, T. J. Freeborn, A. S. Elwakil, M. E. Fouda, B. J. Maundy, A. G. Radwanh, Z. Said, and M. A. Abdelkareem, "Review of fractional-order electrical characterization of supercapacitors." *J. Power Sources*, **400**, 457 (2018).
9. C. Campestrini, P. Keil, S. F. Schuster, and A. Jossen, "Ageing of lithium-ion battery modules with dissipative balancing compared with single-cell ageing." *J. Energy Storage*, **6**, 142 (2016).
10. P. Arora, R. E. White, and M. Doyle, "Capacity fade mechanisms and side reactions in lithium-ion batteries." *J. Electrochem. Soc.*, **145**, 3647 (1998).
11. M. Safari, M. Morcrette, A. Teyssot, and C. Delacourt, "Multimodal physics-based aging model for life prediction of li-ion batteries." *J. Electrochem. Soc.*, **156**, A145 (2008).
12. G. Dong and J. Wei, "A physics-based aging model for lithium-ion battery with coupled chemical/mechanical degradation mechanisms." *Electrochim. Acta*, **395**, 139133 (2021).
13. R. Kötz, P. Ruch, and D. Cericola, "Aging and failure mode of electrochemical double layer capacitors during accelerated constant load tests." *J. Power Sources*, **195**, 923 (2010).
14. F. Naseri, E. Farjah, M. Allahbakhshi, and Z. Kazemi, "Online condition monitoring and fault detection of large supercapacitor banks in electric vehicle applications." *IET Electr. Syst. Transp.*, **7**, 318 (2017).
15. M. He et al., "Ageing phenomena in high-voltage aqueous supercapacitors investigated by in situ gas analysis." *Energy Environ. Sci.*, **9**, 623 (2016).
16. F. Hlawatsch and F. Auger, *Time-Frequency Analysis: Concepts and Methods* 1st ed. (2008) (ISTE).
17. Y. Li, K. Li, X. Liu, X. Li, L. Zhang, B. Rente, T. Sun, and K. T. Grattan, "A hybrid machine learning framework for joint soc and soh estimation of lithium-ion batteries assisted with fiber sensor measurements." *Applied Energy*, **325**, 119787 (2022).
18. Z. Geng and T. Thiringer, "In situ key aging parameter determination of a vehicle battery using only can signals in commercial vehicles." *Applied Energy*, **314**, 118932 (2022).
19. P. Wei and H.-X. Li, "Multiscale dynamic construction for abnormality detection and localization of li-ion batteries." *Applied Energy*, **325**, 119814 (2022).
20. M. Uno and K. Tanaka, "Accelerated charge-discharge cycling test and cycle life prediction model for supercapacitors in alternative battery applications." *IEEE Trans. Ind. Electron.*, **59**, 4704 (2011).
21. A. Allagui, A. R. Baboukani, A. S. Elwakil, and C. Wang, "Electrochemical stability analysis of red phosphorus-based anode for lithium-ion batteries." *Electrochim. Acta*, **395**, 139149 (2021).
22. B. Boashash, *Time-Frequency Signal Analysis and Processing: A Comprehensive Reference* (Academic Press) (2015).
23. Y. Qi, L. Yang, B. Liu, L. Liu, Y. Liu, Q. Zheng, D. Liu, and J. Luo, "Accurate diagnosis of lung tissues for 2d raman spectrogram by deep learning based on short-time fourier transform." *Anal. Chim. Acta*, **1179**, 338821 (2021).
24. A. Mertins and D. A. Mertins, *Signal Analysis: Wavelets, Filter Banks, Time-Frequency Transforms and Applications* (Wiley) (1999).
25. A. V. Oppenheim, R. W. Schafer, and J. R. Buck, *Discrete-Time Signal Processing* 2nd ed.(Prentice Hall) (1999).
26. G. E. Box, G. M. Jenkins, G. C. Reinsel, and G. M. Ljung, *Time Series Analysis: Forecasting and Control* (Wiley) (2016).